Structures and Thermodynamic Stability of Cobalt Molybdenum Oxide ($CoMoO_4$-II)

Ibrahem S. Altarawneh , Saleh E. Rawadieh ,
Mohammad A. Batiha , Leema A. Al-Makhadmeh ,
Mouath A Al-Shaweesh , Mohammednoor K. Altarawneh

PII: S0039-6028(18)30325-X
DOI: 10.1016/j.susc.2018.05.018
Reference: SUSC 21269

To appear in: *Surface Science*

Received date: 15 April 2018
Revised date: 27 May 2018
Accepted date: 29 May 2018

Please cite this article as: Ibrahem S. Altarawneh , Saleh E. Rawadieh , Mohammad A. Batiha , Leema A. Al-Makhadmeh , Mouath A Al-Shaweesh , Mohammednoor K. Altarawneh , Structures and Thermodynamic Stability of Cobalt Molybdenum Oxide ($CoMoO_4$-II), *Surface Science* (2018), doi: 10.1016/j.susc.2018.05.018

Highlights

- Estimated properties of bulk $CoMoO_4$-II reproduce limited analogous experimental measurements.
- Upward displacement of surface oxygen atoms is observed in most optimized surfaces.
- Mo/Co-O bonds display an ionic character.
- O-truncated surfaces dominate the thermodynamic stability trend.

Structures and Thermodynamic Stability of Cobalt Molybdenum Oxide ($CoMoO_4$-II)

Ibrahem S. Altarawneh[1], Saleh E. Rawadieh[2,3]Mohammad A. Batiha[2], Leema A. Al-Makhadmeh[4], Mouath A Al-Shaweesh,[4] Mohammednoor K. Altarawneh[2,5*]

[1] Pharmaceutical and Chemical Engineering Department, German Jordanian University, Amman 11180, Jordan)

[2]Chemical Engineering Department, Al-Hussein Bin Talal University, Ma'an, Jordan

[3]Renewable Energy Research and Development Center, Al-Hussein Bin Talal University, Ma'an, Jordan

[4]Environmental Engineering Department, Al-Hussein Bin Talal University, Ma'an, Jordan

[5]School of Engineering, Murdoch University, 6155, WA, Australia

*Corresponding author: Email: M.Altarawneh@Murdoch.edu.au

Abstract

This contribution reports density functional theory (DFT) calculations on structural and electronic properties of bulk and surfaces of cobalt molybdenum oxide $CoMoO_4$-II; i.e., a material that enjoys a wide array of chemical catalytic and optical applications. Estimated lattice constants and atomic charges for bulk $CoMoO_4$-II reproduce limited analogous experimental measurements. Bader's charges confirm the ionic nature for metal-O bonds in bulk and surfaces of $CoMoO_4$-II. Plotted partial density of states reveal a narrow band gap of 1.8 eV for bulk $CoMoO_4$-II. We found that cleaving bulk of $CoMoO_4$-II along the low-Miller indices afford twelve distinct surfaces. Upward displacement of oxygen atom becomes evident when contrasting bulk positioning of atoms with relaxed surfaces. The two mixed Mo/O- and Co/O--terminated surfaces dominate the thermodynamic stability diagram at 1 atm and 300 – 1400 K, and across a wide range of oxygen chemical potential. The presence of surface oxygen atoms in these stable surfaces is expected to facilitate the occurrence of oxygen reduction reactions as experimentally demonstrated. Likewise, the adjacent surface cations (Mo^{4+}/Co^{2+}) and anions (O^{2-}) serve as Lewis-acid pairs; i.e., very potent active sites in prominent catalysis reactions.

Keywords: $CoMoO_4$-II; lattice constants; DFT + U; Surfaces; Thermodynamic stability

1. Introduction

Owing to unique structural and electronic properties, binary transition metal oxides (BTMOs) have enjoyed prominent applications in strategic areas spanning supercapacitors, electrochemical reactions and catalysis.[1] Of particular importance are cobalt molybdenum oxide ($CoMoO_4$) – based materials. They are being deployed in mobile communication systems and high-quality microwave dielectric ceramics and in applications pertinent to harsh operating conditions. The high-temperature β-phase of $CoMoO_4$ has been utilized in numerous catalytic applications such as degradation of organic dyes,[2] dehydrogenation, hydrocracking of camelina, hydrogenation of unsaturated hydrocarbons, hydrodesulfurization (HDS) of thiophene,[3] reduction of nitrophenol isomers, water-splitting reactions[4] and oxygen reduction reactions.[5] For instance, Al-Wadaani et al.,[6] reported rapid conversion of nitrophenols to their corresponding aminophenol's via reaction rate constants in the range of 0.27 – 1.3 min^{-1}. Sheets of bimetallic CoMo were shown to support growth of CNTs and to serve as potential replacements of Pd-catalysis for HDS reactions.[7] However, the main applications of $CoMoO_4$-based materials are in the areas of energy storage and supercapacitors. Stemmed from remarkable redox reactions afforded by $CoMoO_4$, it generates effective capacitive measurements at 326 F g^{-1} while retaining 95% of the capacitance after 10000 cycles [8]. Several studies report the outstanding electrochemical performance of $CoMoO_4$ in which it works as the supercapacitor electrode and exhibits a profound specific capacitance and exceptional recycling stability[1].

The Faradic mechanism driven by $CoMoO_4$ is well-documented in the literature [1]. The main redox reaction carried out by $CoMoO_4$ can be expressed as $Co_3O_4 + H_2O + OH^{-1} \rightarrow 3CoOOH + e^{-1}$. In addition to neat $CoMoO_4$, supercapacitors constructed from nanohoneycomb-like strongly coupled $CoMoO_4$–graphene electrodes was shown to deliver super-long-life performance [9]. However, transition metal oxides in general are known to act as precursors for the formation of notorious pollutants [10-12].

$CoMoO_4$ is synthesized by various methodologies including, gas-solid state reactions (i.e., chemical synthesis), electrospinning, microwave synthesis, evaporation/condensation of a

polymer-based metal-complex precursor mixtures, sol–gel and micro-emulsion [13]. The most applied method is the so-gel method because it offers controllable purity in terms of composition, homogeneity and porosity. These structural parameters can readily be altered with the temperature [14]. However, application of this method for a large-scale synthesis of $CoMoO_4$ is generally hindered in view of the requirements of large quantities of inorganic solution precursors, surfactants and solvents. A facile hydrothermal method was recently deployed to produce CoMoO4 nanoparticles/graphene composites for energy storage applications.

The $CoMoO_4$ bulk unit cell exists in three phases; i.e., α, γ and β.[15,16]. The β-phase adapts the P_2/c space group and it differs from the α-phase in the coordination of the Mo^{6+} ions that occupy tetrahedral positions. The γ-phase appears at the high pressure and crystalizes in $NiWO_4$ structure type along with the space group C_2/m. Using the self-propagating room temperature procedure (SPRT), Zagorac et al. [16] synthesized two configurations of $CoMoO_4$; termed as (I) and (II). The II phase was shown to correspond to the high-pressure configuration. Via deploying empirical potentials, the authors screened for the existence for other theoretically potential phases pointing out to eleven accessible phases. I- and I-phases are isosymmetric polymorphs (both shares the same *C2/m* space group). The irreversible I → II transition was observed in a DSC experiment at temperature as low as ~ 700K via an accessible transition enthalpy of only 46.8 J/g.[17].

To the best of our knowledge, literature presents no atomic-scale description based on DFT calculations for any of the $CoMoO_4$ phases or for any of its low-Miller indices surfaces. Herein we report DFT account on structural and electronic properties for the high-pressure phase of bulk $CoMoO_4$-II and all surface plausible configurations of this phase. This study has a twofold aim, (*i*): to report the thermodynamically most stable structure of $CoMoO_4$-II and (*ii*) to provide atomic-based insight into the unique catalytic and energy storage properties of $CoMoO_4$.

2. Computational details

2.1.Structural optimizations

VASP package [18] carried out geometries optimizations and energy calculations for bulk $CoMoO_4$-II and its low-Miller indices surfaces within the formalism plane wave DFT. The computational methodology comprises spin-unrestricted PAW-GGA functional [19], Grimme's van der Waals dispersion correction [20], a cutoff energy of 450 eV, and a dipole correction applied in the z-direction (only for surfaces) to compensate for any developed dipole momentum in the vertical direction. The unit cell of $CoMoO_4$-II was optimized using a cutoff energy of 500 eV with a κ-points sampling of 8 × 8 × 8.

The presence of *d* orbitals in Mo and Co atoms necessitates the inclusion of the Hubbard term [21], $U_{eff} = U - J$. The *U* term accounts for the strong one-site Coulomb interaction of *d* orbitals while the *J* terms accounts for the repulsion of opposite spin electrons. An appropriate U_{eff} value stems from parametrization against experimentally measured parameters; most notable the electronic band gap. Bulk [22] and nanorods [23] of $CoMoO_4$ feature a narrow band gap of 1.8 – 2.0 eV. We found that pure DFT wrongly produces a metallic character of bulk $CoMoO_4$-II and that the band gap starts to open at ~ U_{eff} = 3.0 eV for both Mo and Co atoms. A U_{eff} value at 8.0 eV for both atoms reproduces the lower limit of the available experimental values of the band gap; i.e., 1.8 eV. Accordingly, all surface calculations are carried out with considering a U_{eff} value of 8.0 eV.

Surfaces of $CoMoO_4$-II were constructed based on symmetric slabs that composed of 2 × 2 unit cell separated by at least 10 Å vacuum region separating the periodic images on both sides of the slabs. Slabs contain 8-12 layers with 46-60 atoms. Integration of the Brillouin zone was performed using automatic mesh κ- generation[24] of 4 × 4 × 1 and 3 × 4 × 1 for 100 and 110/111 surfaces; respectively. A test on one structure using a 5 × 5 × 1 and 500 eV changed its total energy by only 50 meV. Structures were allowed to relax with convergence criteria of energy and force tolerance on each atom converged to less than 10^{-5} eV and 10^{-2} eV/Å for total

energy and force on each atom; respectively. Atomic charges for bulk and surfaces $CoMoO_4$-II were evaluated based on Bader's formalism [25] that partitions the electronic density into partial localized electronic charges.

2.2. Ab initio atomistic thermodynamics

Literature [26,27] provides detailed description of equations underlying the ab initio atomistic thermodynamics approach. In this formalism, the surface energy $\gamma(T, P)$ varies with the chemical potential $\mu_i(T, P)$ of the atomic constituent i according to:

$$\gamma(T,P) = \frac{1}{2A}(G(T,P) - \sum_i N_i \mu_i(T,P)) \quad \text{(Eq1)}$$

in which $G(T, P)$ represents the Gibbs free energy of the slab, A stands for the surface area of the slab, and N_i denote the atom numbers in the slab for component i. Thus for the slabs of $CoMoO_4$-II , the surface free energy equation is expressed as:

$$\gamma(T,P) = \frac{1}{2A}(G_{\text{slab}}(T,P) - N_{Co}\mu_{Co}(T,P) - N_{Mo}\mu_{Mo}(T,P) - N_o\mu_o(T,P)) \quad \text{(Eq2)}$$

It has been shown that, the Gibbs free energy term of the surfaces changes only marginally with temperature and pressure [27] and thus, $G_{\text{slab}}(T,P) = G_{\text{slab}}(0\text{ K}, 0\text{ atm})$. Chemical potential for the three atomic components is the summation of the change in chemical potential and total energies of Co (taken as the energy of bulk Co per unit formula), Mo (taken as the energy of bulk Mo per unit formula) and O atom (taken as 0.5 of the energy of an oxygen molecule):

$$\begin{aligned}
\mu_{Co}(T,P) &= \Delta\mu_{Co}(T,P) + E_{Co} \\
\mu_{Mo}(T,P) &= \Delta\mu_{Mo}(T,P) + E_{Mo} \\
\mu_O(T,P) &= \Delta\mu_O(T,P) + \frac{1}{2}E_{O_2}
\end{aligned} \quad \text{(Eq3)}$$

The T-P change in chemical potential signifies the difference in enthalpies (H) and entropies (S). The latter two quantities are sourced from NIST-JANAF [28] tables:

$$\Delta\mu_{Co}(T,P) = [H_{Co}(T,P^o) - H_{Co}(T^o,P^o)] - T[S_{Co}(T,P^o) - S_{Co}(T^o,P^o)] + kT\ln\frac{P}{P^o}$$

$$\Delta\mu_{Mo}(T,P) = [H_{Mo}(T,P^o) - H_{Mo}(T^o,P^o)] - T[S_{Mo}(T,P^o) - S_{Mo}(T^o,P^o)] + kT\ln\frac{P}{P^o} \quad \text{(Eq4)}$$

$$\Delta\mu_{O}(T,P) = \frac{1}{2}[H_{O_2}(T,P^o) - H_{O_2}(T^o,P^o)] - \frac{T}{2}[S_{O_2}(T,P^o) - S_{O_2}(T^o,P^o)] + \frac{1}{2}kT\ln\frac{P}{P^o}$$

Figure S.1 in the supplementary materials presents **c**hange in chemical potentials for Mo, Co and O at 1 am and change in chemical potential for Mo at various pressures. The deployed surface energy equation utilizes values of chemical potentials for the three elements as a function of temperature and pressure.

3. Results and Discussions

3.1. Bulk of $CoMoO_4$-II

Figure 1 shows the optimized geometries of bulk $CoMoO_4$-II while Table 1 contrasts prominent calculated structural and electronic parameters with their analogous experimental estimates. The unit cell of $CoMoO_4$-II exhibits a fourfold coordination of Mo^{6+} ions by O^{2-} anions in a tetrahedral arrangement and a six-fold coordination of Co^{2+} cations by O^{2-} anions in an octahedral environment along the space group of *C2/m* space group. Computed lattice constants deviate from their corresponding experimental measurements in the range of 2.3 – 3.7%. Calculated Mo-O (1.797 Å) and Co-O (1.979 Å) distances differ from their analogous experimental measurements by only 0019 Å and 0.122 Å, respectively. Likewise, the two calculated O-O spacings (2.676 Å and 2.872 Å) deviate from XRD values by only 0.019 Å and 0.047 Å. Livage et al.[15] estimated atomic charges via the bond valence method. Predicted charges by Livage et al.[15] underestimate computed Bader's charges in this work (Table 1); nonetheless, both approaches indicate an ionic nature for Mo/Co-O bonds in bulk $CoMoO_4$-II. Higher positive charges on Mo atoms (3.97 *e*), in reference to Co (1.44 *e*) indicate stronger Mo-O bonds than Co-O bonds.

The density of states (DOS) and partial DOS plots shown in Figure 2.a features narrow band of around 1.8 eV, in a close agreement with experimental measurements. The upper valance band mainly consists of O(*p*) and Co(*d*) orbitals while the conduction band is mainly composed of Mo(*d*) orbitals. Finally, we calculate the Gibbs free energy (G^f_{Bulk}) of formation for bulk $CoMoO_4$-II (per unit formula) at 1 atm based on:

$$G^f_{Bulk} = G_{Bulk}(0\text{ K, }0\text{ atm}) - \mu_{Co}(T,1\text{ atm}) - \mu_{Mo}(T,1\text{ atm}) - 4\mu_O(T,1\text{ atm})$$

Figure 3 shows the change in G^f_{Bulk} values with temperature at 1 am. At 298.1 K, the calculated G^f_{Bulk} amounts to -5.1 eV. Formation of bulk of $CoMoO_4$-II appears to be spontaneous up to 1200 K. To the best of our knowledge, literature presents no analogous either experimental or theoretical value to compare with.

3.2. Low-Miller index surfaces of $CoMoO_4$-II.

We consider all low-Miller-index orientations of $CoMoO_4$-II configurations along the (001), (010), (100), (011), (101), (110) and (111) directions with all possible atomic-surface terminations. Initially, there were six different surface terminations, but following full optimizations, only twelve distinct surfaces were obtained. Figures 4 and 5 present the optimized minimum energy structure of the twelve considered surfaces while Table 2 enlists their atomic compositions. Surfaces are termed based on their and surface top-most elemental compositions (in the optimized geometries) and planar orientations. For instance, the 111_CoMoO surface represents a construction truncated along the [111] direction with Co/Mo/O atoms located in the outmost layer, in sequential. Contrasting the atomic-type terminations between initial and final optimized geometries reveal significant relaxations in many configurations. For example, truncating the bulk structure along the [100] direction initially affords Mo-and Co terminated surfaces, however, the final relaxed structures experienced upward movements of oxygen atom. The optimized structures display mixed Mo/O and Co/O mixed terminations in the upmost atomic layers. Figure 6 displays the oxygen upward movements pertinent to 100_MoO and 100-CoO surfaces. The upward displacement of

electronegatively charged atoms in transition metal oxides were also observed in $CuCl_2$, $CuBr_2$, $FeCl_2$ and $CoCu_2O_3$ surfaces [10,11,29,30].

The 010 direction encompasses two distinct O-terminated surfaces termed as 010_O(A), 010_O(B) surfaces. These two structures differ by the surface bonding environments as shown in the top panel of Figure 4. Three surfaces include mixed Mo/Co/O terminations in their topmost layers (101_CoMoO, 110_MoCoO and 111_CoMoO). Binary Mo/O or Co/O-truncated surface are featured in 011_MoO, 100_CoO and 100_MoO structures.

Atomic labels in Figures 4 and 5 point out to the compositions of the topmost two-three layers. The 001_O surface consists of sequence of unmixed O, Mo and Co layers. The 010_O(A) and 010_O(B) surfaces comprise stacks of Mo/O and Co/O mixed layers, respectively. The uppermost layers in the 100_O and 110_O structures are composed of dangling Mo-O bonds. Inner atomic layers in the 100_O surface are composed of unmixed Mo, Co and Co layers. The structures of 101_CoMoO and 111_CoMoO surfaces display mixed Co/Mo/O layers.

As seen in Table 2, only three surfaces exist in the stoichiometry state of $CoMoO_4$, i.e., atomic ratio Co:Mo:O = 1:1:4. The non-stoichiometric surfaces are designated as either oxygen rich or deficient. The implications on the stoichiometry and atomic-type terminations on the thermodynamic stability trend will be discussed in the next section. Based on calculated Bader's charges estimated for selected surfaces (listed in Table 3), we found that O atoms slightly deviate from their bulk values (presented in Table 1). Overall, surface O-Mo and O-Co bonds largely retain their bulk ionic characters.

3.3. Thermodynamic stability diagram

From Figure S.1, oxygen incurs the widest variation in $\Delta\mu$ values in comparison to Co and Mo. Thus, it can be inferred that the change in surface energy values for $CoMoO_4$-II surfaces to be most sensitive to $\Delta\mu_O$ values. As it is the case for bulk $CoMoO_4$-II, chemical potential for Mo and Co atoms can be approximated as their total energies at 0 K and 0 atm calculated by DFT + U calculations (i.e., in Eq3, the $\Delta\mu_{Co}(T,P)$ term is minimal in reference to E_{Co}). In general, accessible values of $\Delta\mu_O$ vary between two limits, an oxygen-lean limit denoted by G^f_{Bulk} for bulk $CoMoO_4$-II (i.e., -5.1V at 298.15 from Figure 3) and an oxygen-rich condition taken arbitrary to be 0.0 eV. Literature provides detailed description of the physical rationale behind considering these two limits.[31]. Figure 7.a present surface free energies for the twelve considered surface terminations based on Eq2). Within the accessible range of oxygen chemical potential, four surfaces share very similar values of low surface free energies; namely, the 100_CoO, 100_MoO, 101_CoMoO and 010_O(B) surfaces (Figure 7.b). The Thermodynamic instability of the 110_O and100_O surfaces could be easily attributed to the presence of unsaturated dangling bonds in their topmost layers.

The surface energy equations described in section 2.2 enables to produce a 3D plot thermodynamic stability diagram for $CoMoO_4$-II surfaces as a function in $\Delta\mu_{Co}$, $\Delta\mu_{Mo}$ and $\Delta\mu_O$. However, it is more convenient to express the surface energy values based on temperature and pressure. As section 2.2 illustrates (Eq3 and Eq4), values of the change in chemical potential solely depends on variation in temperature and pressure. Furthermore, most applications of $CoMoO_4$-II occur at the ambient pressure. Thus, herein we calculate surface energy values at 1 atm for a wide range of temperature (300 – 1400 K).

Figure 8.a plots surface free energies for all considered surfaces as a function of temperature at 1 atm. The two binary mixed 100_MoO and 100_CoO surfaces incur very alike thermodynamic stability between 300 and 1400 K. Figure 7.b clearly shows the very insignificant difference in surface energies among these two surfaces. The presence of O atom in the topmost layer of the thermodynamically most stable surfaces would enable $CoMoO_4$-II to undergo oxygen catalytic reactions. It is generally viewed that surfaces with surplus atoms with large electronegativity

(such as Br, O and Cl) [29,30] tend to be more thermodynamically stable. However, the two most stable surfaces are O-deficient terminations. Thus, we envisage that surplus in oxygen content should not a factor behind the profound thermodynamic stability of these surfaces.

We have recently demonstrated that [30,32] that a combination of structural as well as electronic factors contributes to the thermodynamic stability trend. These potential factors may include of surface relaxation and construction (in reference to bulk values), distribution of electronic charges, reduction in the charge in the topmost layer, as well as the overall polarity (i.e., degree of stoichiometry) of the slab. In this regard, the surface polarity for the non-stochiometric surfaces 100_MoO and 100_CoO may contribute to the stability of these two surfaces. Finally, Figure 2.b discloses that the surface 100_CoO shares similar DOS characteristic to its bulk, albeit with a shorter band gap at only 0.80 eV.

4. Conclusions

Calculated structural and electronic properties for bulk $CoMoO_4$-II coincide with corresponding experimental measurements pertinent to lattice parameters, atomic distances and atomic charges. $CoMoO_4$-II displays a metallic character with ionic Co/Mo-O bonds. The variation of chemical potential of Mo and Co atoms is insignificant when contrasted with that of O atoms. The ab initio atomistic thermodynamic approach provides thermodynamic stability ordering for all plausible surfaces that were classified into stochiometric, O-rich and O-deficient terminations. Several surfaces have experienced profound relaxation evidenced by upward displacement of second and third-layer O atoms to the topmost layer. Mixed Mo/O and Co/O-truncated surfaces incur higher thermodynamic stability in reference to O-terminated surfaces. The thermodynamic stability of these two surfaces is in line with prominent catalytic applications of $CoMoO_4$. The presence of surface cations (Mo^{4+} and Co^{2+}) and anions (O^{2-}) would facilitate the occurrence of importance surface-assisted reactions such as production of hydrogen from water dissociation and partial hydrogenation of alkynes. For instance, in the first step in water fragmentation, H atoms are attached to a surface O^{-2} sites while hydroxyl groups (OH) are linked to cations sites.

Similarly, the very narrow band gap of bulk and surfaces of $CoMoO_4$-II underlines its strategic applications in optical and electronic devices as well as in super capacitors.

Acknowledgements

This work was supported by Australian Research Council (ARC). We acknowledge the Pawsey Supercomputing Centre in Perth as well as the National Computational Infrastructure (NCI) in Canberra, Australia for providing the grants of computational resources.

References

[1] Y. Zhang, L. Li, H. Su, W. Huang, X. Dong, J. Mater. Chem. A 3 (2015) 43.

[2] Y. Fan, W. Ma, J. He, Y. Du, RSC Adv. 7 (2017) 36193.

[3] J.n.L. Brito, A.L. Barbosa, J. Catal. 171 (1997) 467.

[4] X. Li, X. Hao, A. Abudula, G. Guan, J. Mater. Chem. A. 4 (2016) 11973.

[5] Z. Yin, Y. Chen, Y. Zhao, C. Li, C. Zhu, X. Zhang, J. Mater. Chem. A. 3 (2015) 22750.

[6] F. Al-Wadaani, A. Omer, M. Abboudi, H. Oudghiri Hassani, S. Rakass, M. Messali, M. Benaissa, Molecules 23 (2018) 364.

[7] E. Soghrati, M. Kazemeini, A.M. Rashidi, K.J. Jozani, Procedia Engineering 42 (2012) 1484.

[8] X. Geng, Y. Ai, G. Shen, Prog. Nat. Sci: Mater Inter. 26 (2016) 243.

[9] X. Yu, B. Lu, Z. Xu, Advanced materials (Deerfield Beach, Fla.) 26 (2014) 1044.

[10] M. Altarawneh, M.W. Radny, P.V. Smith, J.C. Mackie, E.M. Kennedy, B.Z. Dlugogorski, Appl. Surf. Sci. 254 (2008) 4218.

[11] M. Altarawneh, M.W. Radny, P.V. Smith, J.C. Mackie, E.M. Kennedy, B.Z. Dlugogorski, A. Soon, C. Stampfl, J. Chem. Phys. 130 (2009) 184505.

[12] N. Ahubelem, M. Altarawneh, B.Z. Dlugogorski, Tetrahedron Lett. 55 (2014) 4860.

[13] D. Chen, Q. Wang, R. Wang, G. Shen, J. Mater. Chem. A. 3 (2015) 10158.

[14] A. Sen, P. Pramanik, Mater. Lett. 10 (2001) 287.

[15] C. Livage, A. Hynaux, J. Marrot, M. Nogues, G. Ferey, J. Mater. Chem. 12 (2002) 1423.

[16] D. Zagorac, J.C. Schön, M. Rosić, J. Zagorac, D. Jordanov, J. Luković, B. Matović, Cryst. Res. Technol. 52 (2017) 1700069.

[17] M. Knapp, C. Baehtz, H. Ehrenberg, H. Fuess, J. Synchrotron Rad. 11 (2004) 328.

[18] G. Kresse, J. Furthmüller, Physical review B 54 (1996) 11169.

[19] J.P. Perdew, K. Burke, Y. Wang, Phys. Rev. B. 54 (1996) 16533.

[20] S. Grimme, J. Comput. Chem. 27 (2006) 1787.

[21] S.L. Dudarev, G.A. Botton, S.Y. Savrasov, C.J. Humphreys, A.P. Sutton, Phys. Rev. B. 57 (1998) 1505.

[22] P.P. K, N.B. N.S, K.R. B, Indian. J. Pure. Appl. Phys. 44 (2006) 52.

[23] d.M.A. P, d.O. L., P.P. F, R.I. L, L.M. S, L. S, V.J. A, Adv. Chem. Eng. Sci. (2012) 465.

[24] H.J. Monkhorst, J.D. Pack, Phys. Rev. B. 13 (1976) 5188.

[25] G. Henkelman, A. Arnaldsson, H. Jónsson, Comput. Mater. Sci. 36 (2006) 354.

[26] C. Stampfl, Catalysis Today 105 (2005) 17.

[27] J. Rogal, K. Reuter, M. Scheffler, Phys. Rev. B. 69 (2004) 075421.

[28] M.W. Chase, S. National Institute of, Technology, NIST-JANAF thermochemical tables, American Chemical Society ; American Institute of Physics for the National Institute of Standards and Technology, [Washington, D.C.]; Woodbury, N.Y., 1998.

[29] M. Altarawneh, Z.-T. Jiang, B.Z. Dlugogorski, Phys. Chem. Chem. Phys. 16 (2014) 24209.

[30] M. Altarawneh, A. Marashdeh, B.Z. Dlugogorski, Phys. Chem. Chem. Phys. 17 (2015) 9341.

[31] J. Rogal, K. Reuter, M. Scheffler, Phys. Rev. B. 98 (2007) 046101.

[32] H. Widjaja, H.A. Miran, M. Altarawneh, I. Oluwoye, H.N. Lim, N.M. Huang, Z.-T. Jiang, B.Z. Dlugogorski, Mater. Chem. Phys. 201 (2017) 241.

Table 1: Calculated and literature's values of structural parameters and electronic charges for bulk $CoMoO_4$-II.

Lattice parameters (Å)	***a***	***b***	***c***
Calculated	4.493	5.556	4.911
Experimental [15]	4.660	5.686	4.916
Atomic distances (Å)	**Mo-O**	**Co-O**	**O-O**
Calculated	1.794	1.979	2.676, 2.872
Experimental [15]	1.775	2.101	2,695, 2.825
Atomic Charges (*e*)	**O**	**Mo**	**Co**
Calculated	-1.29, -1.41	3.97	1.44
Other calculated [15]	-1.84	5.94	2.04

Table 2: Atomic compositions of $CoMoO_4$-II surfaces. When the summation of Mo and Co atoms exceeds half of the number of oxygen atoms; the surface is termed as O-rich.

Optimized surface	Initial Surface	Slab composition O: Mo: Co	
001_O	001_MoCo	32:7:7	O-rich
010_O(A)	010_MoO	24:6:6	Stochiometric
011_O	011_O	28:6:8	Stochiometric
011_MoO	011_OMo	26:8:6	O-deficient
100_CoO	100_Co	24:6:8	O-deficient
100_MoO	100_MO	16:6:4	O-deficient
100_O	100_O	24:6:4	O-rich
100_MoCoO	110_MoCoO	26:7:7	O-deficient
110_O	110_O	28:6:6	O-rich
111_MoCoO	111_CoMoO	43:12:12	O-deficient
010_O(B)	010-OCo	16:4:4	Stochiometric
110_MoCoO	110_MoCoO	28:6:6	O-rich

Table 3: Electronic charges (in *e*) on surface atoms in some selected terminations.

101_CoMoO	Atomic charge	**100_CoO**	Atomic charge
O1	-0.13	O1	-1.33
Co	1.41	O2	-1.31
Mo	3.98	Co	1.33
010_O(B)		Mo	3.29
O1	-1.38	**100_MoO**	
O2	-1.33	O1	-1.44
Co	1.43	O2	-1.43
Mo	4.1	Co	1.31
101_O		Mo	2.29
O1	-1.21	**011_MoO**	
O2	-1.29	O1	-1.25
Co	2.1	Co	2.2
Mo	3.9	Mo	3.8

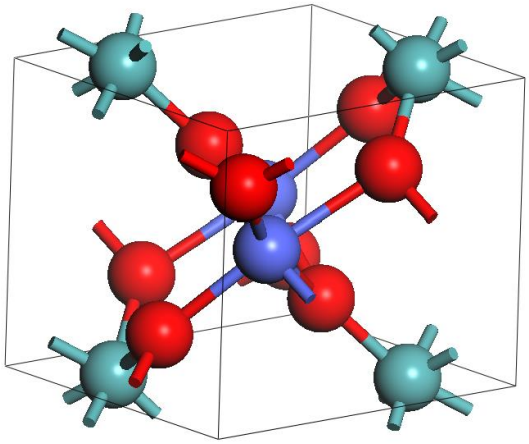

Figure 1: Unit cell of bulk $CoMoO_4$-II. Red, blue and green spheres denote O, Co and Mo colors; respectively.

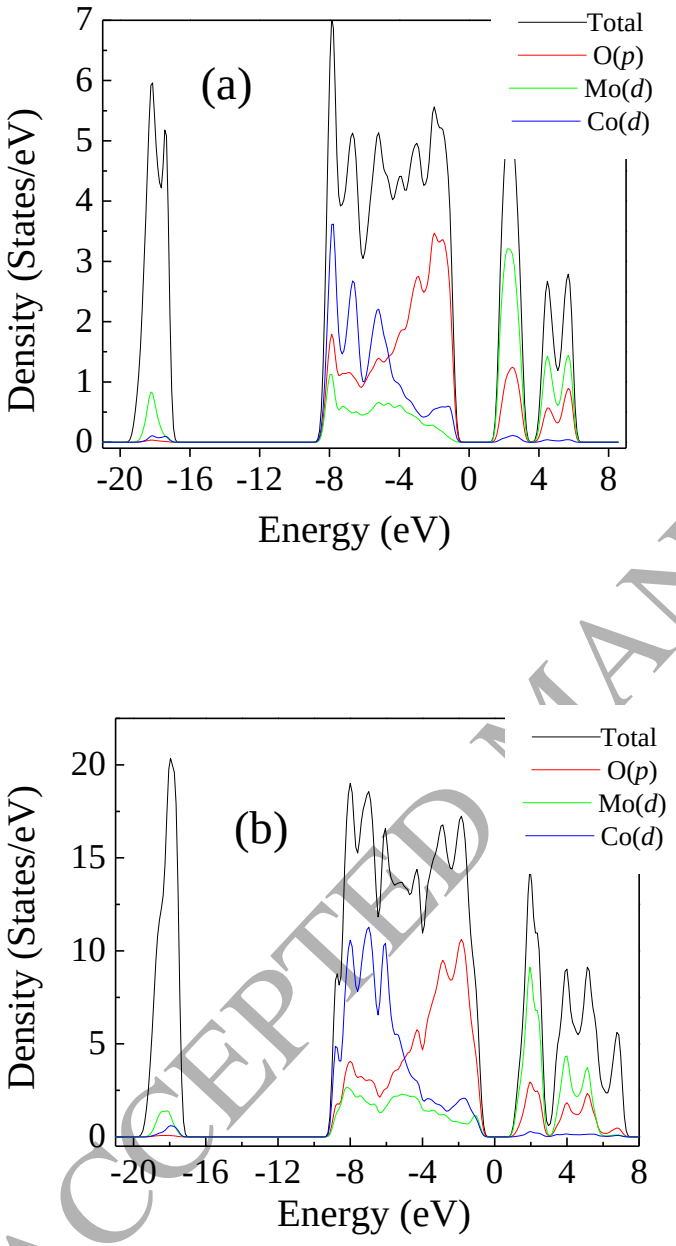

Figure 2: DOS and PDOS for bulk $CoMoO_4$-II (a) and for the 100_CoO surface (b). The Fermi level is set at 0 eV.

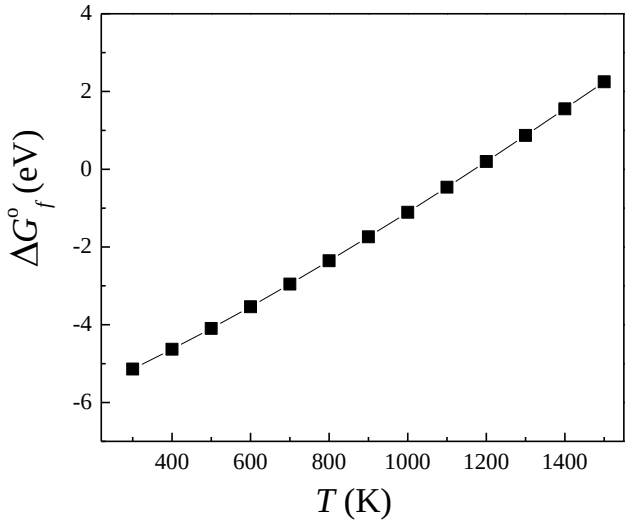

Figure 3: The change in G^{f}_{Bulk} values for bulk $CoMoO_4$-II with temperature at 1 am.

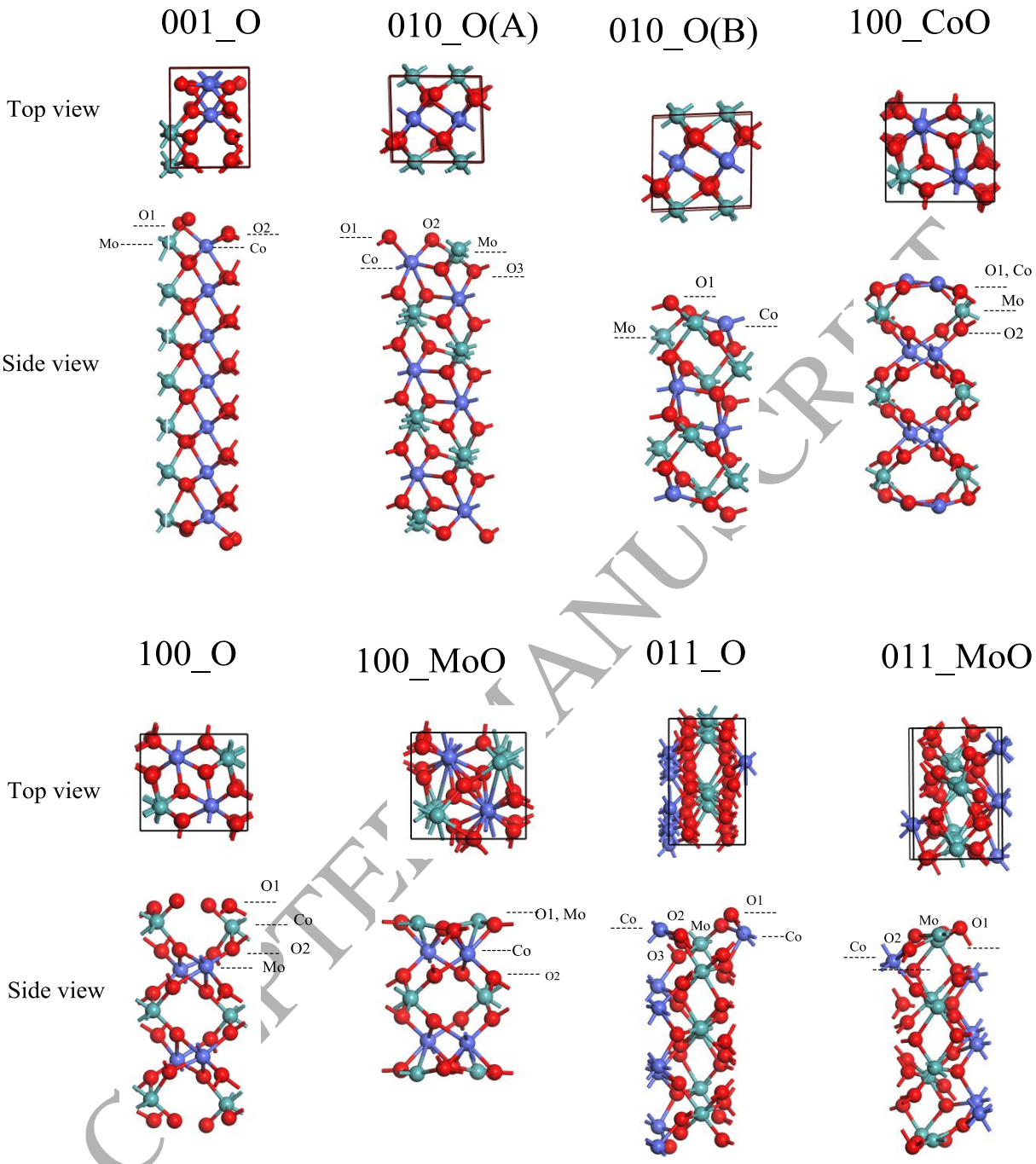

Figure 4: Optimized surfaces of $CoMoO_4$-II. Red, blue and green spheres denote O, Co and Mo colors, respectively.

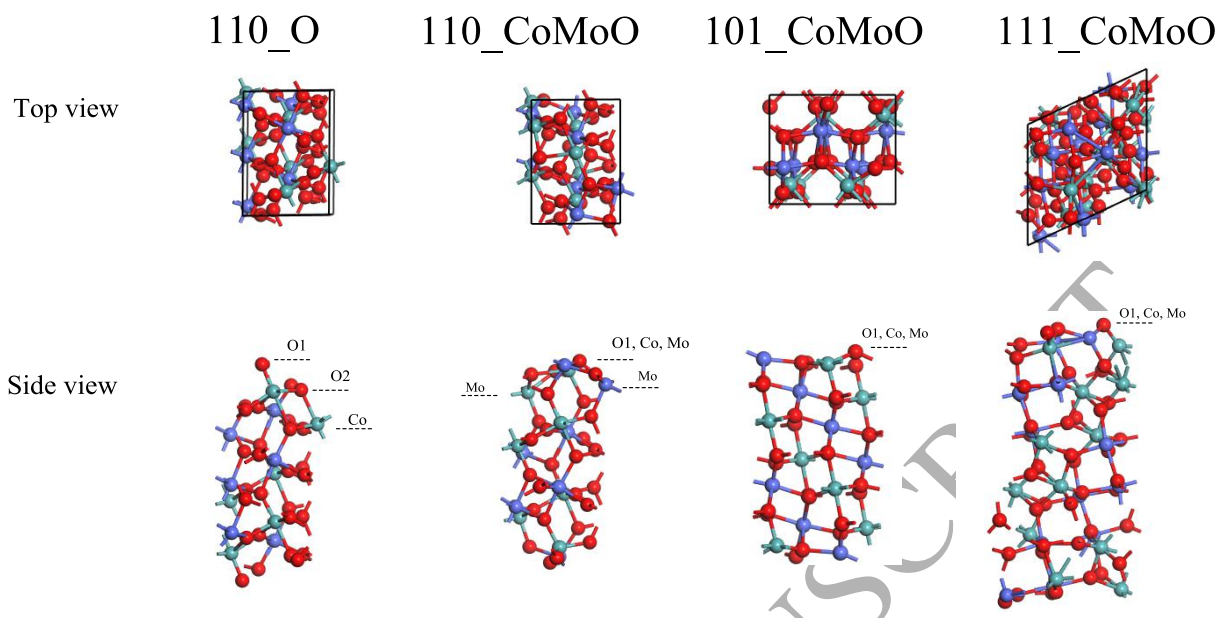

Figure 5. Optimized surfaces of $CoMoO_4$-II. Red, blue and green spheres denote O, Co and Mo colors; respectively.

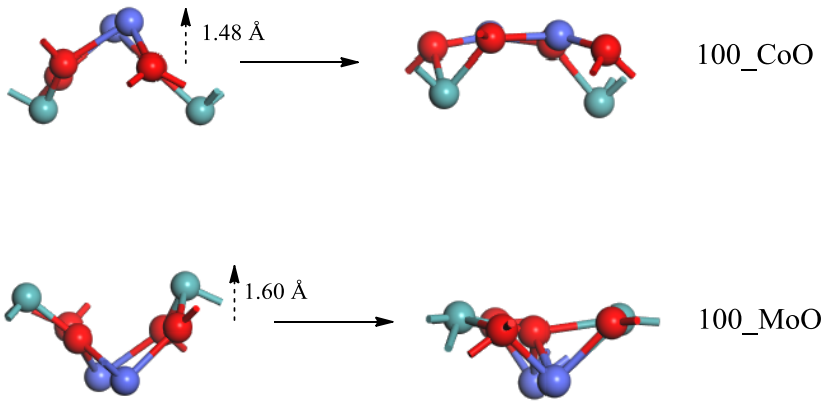

Figure 6. Structural changes encountered during optimization of 100_CoO and 100_MoO surfaces.

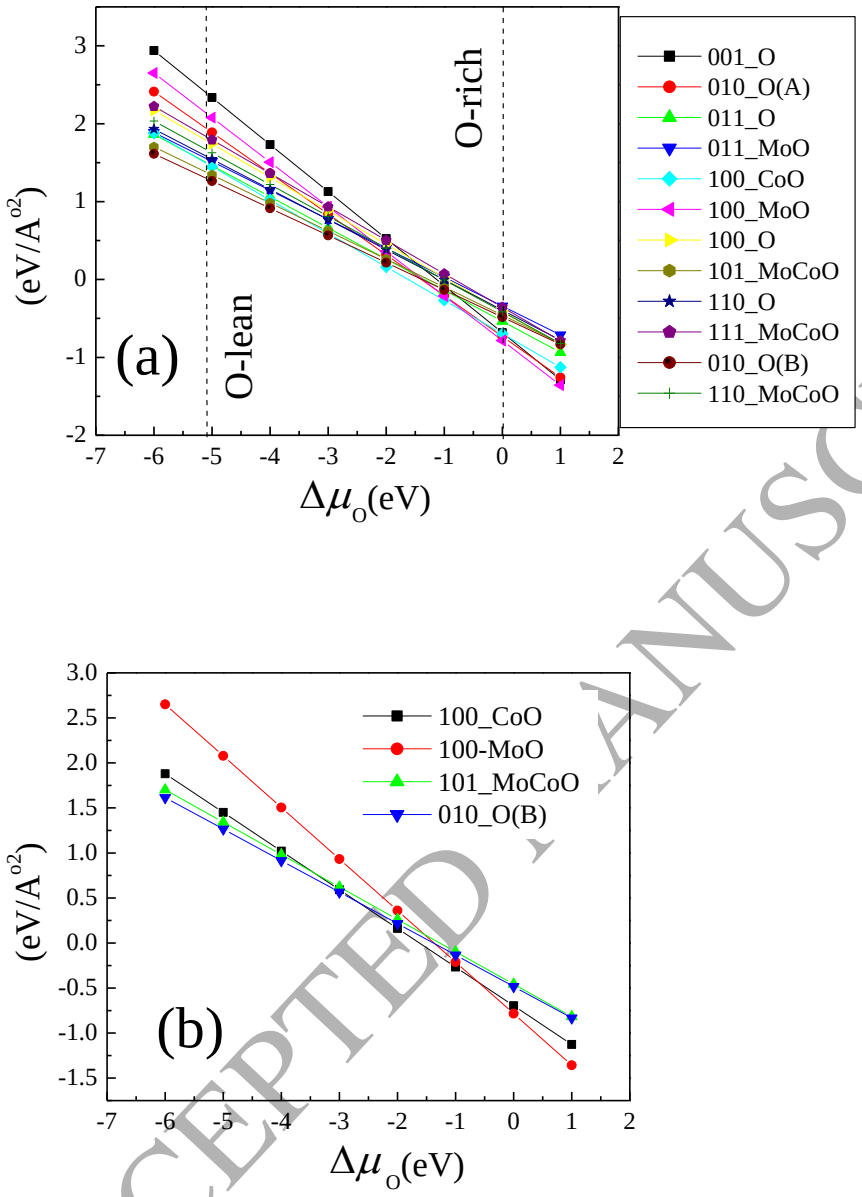

Figure 7: Surface free energies for all plausible terminations (a), and for the thermodynamically two most stable surfaces (b), as a function of oxygen chemical potential.

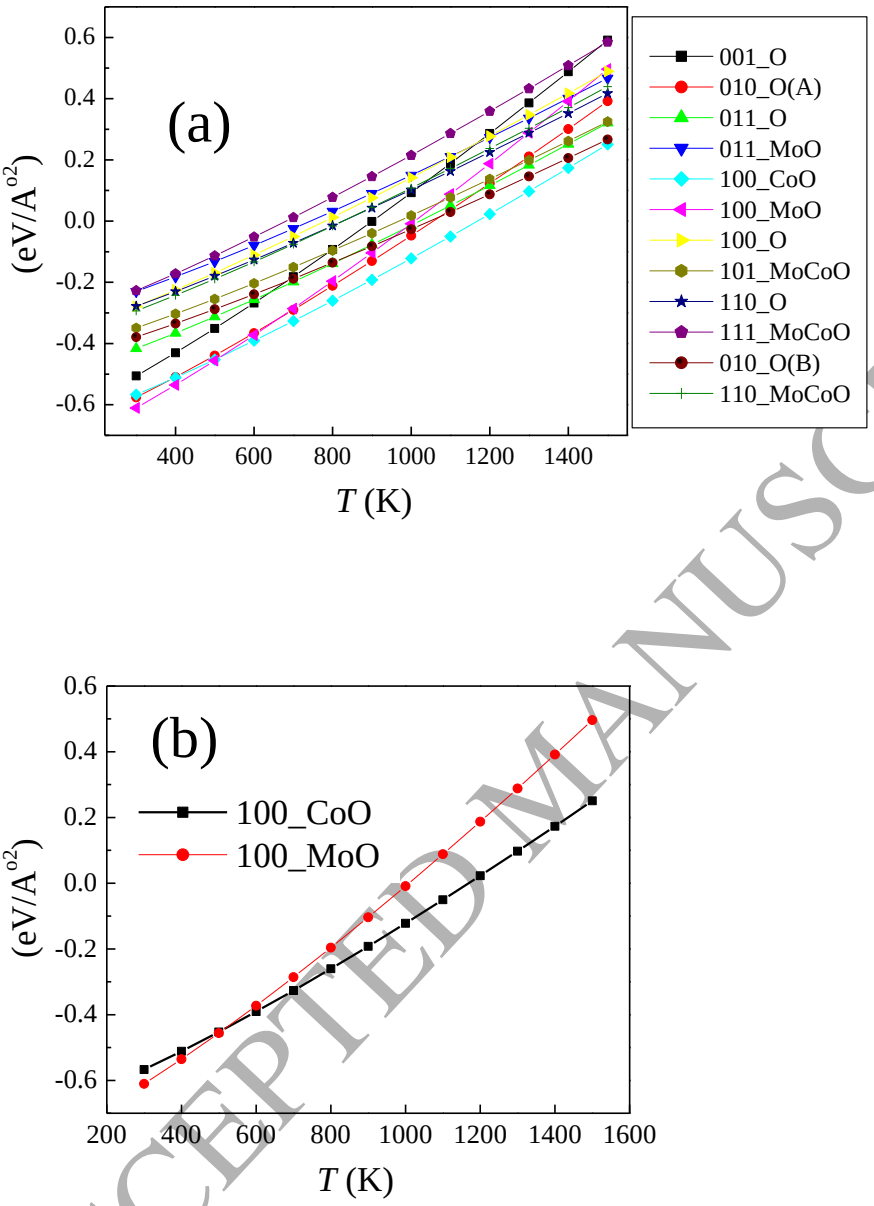

Figure 8: Surface free energies for all plausible terminations (a), and for the thermodynamically two most stable surfaces (b), as a function of temperatures at 1 atm, with considering the chemical potentials for the three elements.

Graphical Abstract